Journal of Science and Technology in Civil Engineering, HUCE, 2023, 17 (3): 114–127

AN ANALYTICAL APPROACH TO PREDICT POST-CRACKING BEHAVIOR OF STEEL FIBER REINFORCED CONCRETE CONSIDERING THE FIBERS ORIENTATION

Vu Chi Cong[a,*], Vu Duc Tam[b]

[a]*Faculty of Building and Industrial Construction, Hanoi University of Civil Engineering, 55 Giai Phong Road, Hai Ba Trung District, Hanoi, Vietnam*
[b]*Université Gustave Eiffel, 14 Boulevard Newton, Champs-sur-Marne, 77420, Marne la Valée, France*

Article history:
Received 10/4/2023, Revised 02/6/2023, Accepted 12/6/2023

Abstract

The presence of steel fiber in plain concrete improves significantly the stiffness as well as the ductility of the material. However, the mechanical behavior in the post-cracking stage of steel fiber-reinforced concrete depends on many factors. Among them, the orientation of the fibers is an important factor that is difficult to quantify. This paper presents a theoretical study that describes the fiber bridging mechanism under tensile stress using a closed-form analytical function. This proposed analytical model allows estimating the stress at a crack opening where the fiber orientation is represented by a Gaussian-like periodic distribution function. The relevance of the proposed model is validated through several numerical analyses with both pre-defined values of different material properties and geometrical parameters of the fibers and the experimental parameters of the two direct tensile tests reported in the literature. The model shows an overall reasonable estimation and presents a lot of potential for further development.

Keywords: steel-fiber-reinforced concrete (SFRC); fiber orientation; pullout mechanism; micromechanics; numerical modeling.

https://doi.org/10.31814/stce.huce2023-17(3)-09

1. Introduction

The concept of enhancing the ductility of concrete by incorporating steel fibers has garnered significant interest in both the scientific community and industrial production. Over the past three decades, the steel fiber-reinforced concrete (SFRC) has expressed its benefits from numerous studies and practical applications [1–4].

In general, when a crack forms, the steel fibers located in the crack zone absorb a portion or all the stress and then redistribute the internal forces through a process known as *pull-out* process, resulting in a reduction of the development of the crack in terms of both size and speed. Experimental studies [5, 6] have shown that with a suitable and well-distributed volume, steel fibers can partially or fully replace conventional steel reinforcement in reinforced concrete structures. This not only provides economic benefits by saving time and labor in the production of steel reinforcement but is also a prerequisite for manufacturing structural elements using 3D printing technology.

The functionality of steel fibers in SFRC is influenced by various factors such as the geometry of the fibers as well as their distribution and orientation within the structure. While the shape, the quantity, and the distribution of fibers can be controlled by formula selection and/or manufacturing methods [7] the orientation of fibers within concrete is a difficult-to-control factor both before and after casting. The orientation of steel fibers has a significant impact on the post-cracking behavior

*Corresponding author. *E-mail address:* congvc@huce.edu.vn (Cong, V. C.)

of SFRC. For instance, experimental results in [8, 9] demonstrated that concrete specimens with a majority of steel fibers oriented along the principal tensile stress direction increase the post-cracking strength. This allows the specimens to withstand considerable stress at high deformation levels. In contrast, when most steel fibers are oriented perpendicular to the principal tensile stress direction, the strength of the material is not strengthened, and brittle failure may occur. Many studies (e.g. [10–12]) have indicated that when the average angle of the fiber with respect to the pulling axis, φ_0, is relatively large ($\varphi_0 \rightarrow 90^\circ$), the pulling force can cause local cracking of the concrete around the fiber or break the fiber before the entire fiber is pulled out. On the other hand, when φ_0 is relatively small ($\varphi_0 \rightarrow 0^\circ$), the fiber pulled-out process can be prolonged, helping to release more energy and produce significant stresses at high level of crack opening.

Regarding the pull-out mechanism of individual fibers, several models have so far been proposed. For instance, Naaman et al. [13] assumed that the initial bond stress between steel fibers and hardened concrete matrix is an empirical constant, and the pulling force of straight fibers parallel to the tension force is determined by the equation of force balance. This model was later developed by Alwan et al. [14] for hooked-end fibers, where the steel fibers are assumed to reach the plastic state after surpassing the debonding stage, and the bending points at the hooks is simulated as a frictional pulley system, from which the generated force due to straightening of the hook can be calculated. Lin et al. [15] proposed an analytical model that takes into account the elastic deformation of straight fibers during the debonding process. This model was further supplemented by the effect of inclined fiber bending at the crack by Zhang et al. [16], and the local concrete crushing effect due to the reaction force at the bending point in [17, 18]. Although this model was only applied to synthetic fibers, it has great potential for further development and application to steel fibers.

So far, numerical studies on the influence of fiber orientation on the post-cracking behavior of fiber-reinforced concrete are still quite limited. For this subject, two main directions can be mentioned: the micromechanical model and the explicit discontinuous model. In the explicit discontinuous model [19, 20], fibers are simulated with specific orientations by special discrete elements. These elements are added to the mesh following the probability distribution function and activated when the stress reaches a critical value. Although these models can provide relatively accurate results and predict the location and the development of cracks, they are highly sensitive to the mesh size and require a very high computation time, especially for complex structures or loads. The micromechanical models [21–24] consider the influence of fiber orientation as a factor that reduces the tensile strength of individual fiber. Although this method may not accurately reflect all physical mechanisms, it has proven highly effective in finite element analysis applications.

Based on the micromechanical model proposed in [21], the present study proposes an analytical function to estimate the tensile stress across the crack. This enables us to develop an effective numerical model that allows representing the post-cracking behavior of steel-fiber reinforced concrete with consideration to the influence of fiber orientation. For this work, the tension force of a steel fiber inclined from the concrete is firstly built based on the combination of the pulley friction model [14] and the elastic deformation model [15]. Then, the fiber orientation factor is calculated through a statistical function. The tensile stress at the crack surface is defined as the sum of the normalized tension forces of all fibers adjusted by the fiber orientation factor. In the present paper, the variations of the proposed model with different material properties and different geometrical parameters are quantified through a parametric study. Additionally, the accuracy of the model is evaluated by comparing its results with the data of two direct tensile tests on SFRC samples collected from the literature.

2. Definition of analytic model

This study focuses on two common types of steel fibers: straight steel fibers and hooked-end steel fibers. The former type is normally used in high-performance concrete, while the latter ones are typically used with conventional concrete in load-bearing structures such as industrial floors, tunnel linings, and drainage culverts [1, 7].

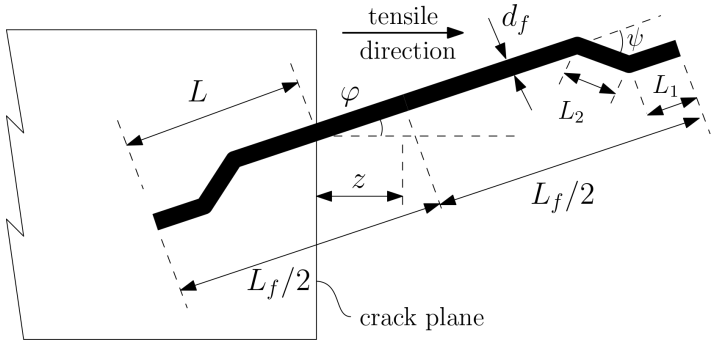

Figure 1. Schema of a single fiber under a crack opening

2.1. *Description of the pullout mechanism of individual fiber*

To illustrate the pullout mechanism of individual steel fiber, a sketch of a hooked-end steel fiber with the length L_f, diameters d_f, length of two hooks L_1 and L_2, and angle between them ψ under a crack opening within a hardened concrete matrix is considered in Fig. 1. It is noted that the straight fiber does not have hooks (i.e. $L_1 = L_2 = 0$). At the time t, there is a crack with a width of w across the position of the steel fiber. The inclination angle of fiber with respect to the crack normal direction is φ and the distance between the middle of fiber and the crack plane is z. The length of embedded part of fiber (L) is given by:

$$L = \frac{L_f}{2} - \frac{z}{\cos\varphi} \tag{1}$$

Generally, the pullout mechanism of steel fibers consists of the following three stages: The first stage is called "debonding stage" (Fig. 2(a)) that the chemical bond between the fiber and the hardened concrete matrix is gradually broken under the tensile force. When all the outer surface of the embedded part is debonded, the second stage called "straightening stage" begins (see Fig. 2(b)). In this stage, the parts of the fiber not parallel to the tensile force will bend, while the part that is straightened will slide. The bending force of non-straight part causes the local compressive reaction on the concrete around the fiber. This force may stretch the fiber beyond the elastic limit. Finally, the fiber will pull out of the concrete with a friction coefficient smaller than the initial steel/concrete friction coefficient in the stage called "frictional slipping" (Fig. 2(c)).

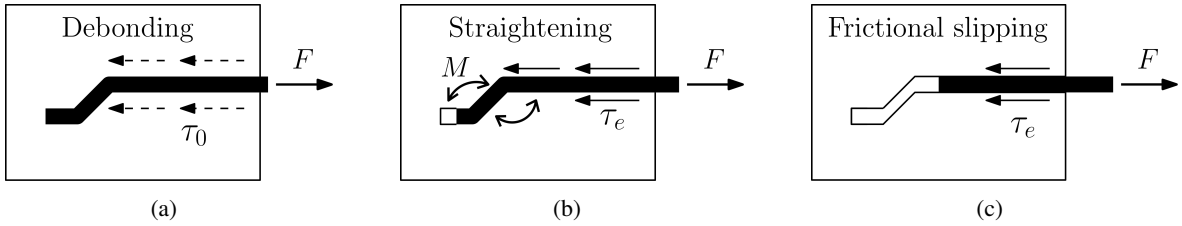

Figure 2. Pullout mechanism of a single fiber

In debonding stage, let λ be the length of the embedded part that has been pulled out, the bridging force (N_d) is the sum of the pullout force on fiber (N_{df}) and the reaction force (N_{dm}) of concrete acts on the outer face of fiber along the length of λ:

$$N_d = N_{df} + N_{dm} \tag{2}$$

The elastic deformation of steel fiber is equal to the elastic deformation of surrounding concrete:

$$\varepsilon_{df} = \varepsilon_{dm} \Leftrightarrow \frac{\sigma_{df}}{E_f} = \frac{\sigma_{dm}}{E_m} \Leftrightarrow \frac{N_{df}}{A_f}\frac{1}{E_f} = \frac{N_{dm}}{A_m}\frac{1}{E_m} \tag{3}$$

$$\Rightarrow N_{df} = \frac{A_f}{A_m}\frac{E_f}{E_m}N_{dm} = \frac{V_f}{V_m}\frac{E_f}{E_m}N_{dm} = \frac{v_f}{1-v_f}\frac{E_f}{E_m}N_{dm} \tag{4}$$

where A_f the cross-sectional area of steel fiber, A_m the sectional area of concrete contributed to tensile strength, E_f, E_m are respectively the Young modulus of steel fiber and concrete matrix, and v_f is the fiber content.

Let $\tau(u)$ be the bond strength between the fiber and the hardened concrete matrix (shortly called concrete in the following paragraph) at position u from the crack to bonded zone ($u \in [0, \lambda]$), the reaction force of surrounding concrete is expressed as follows:

$$N_{dm} = \pi d_f \int_0^{\lambda} \tau(u)du \tag{5}$$

Set $\eta = \frac{E_f}{E_m}\frac{v_f}{1-v_f}$, this coefficient represents the zone where the pullout process of the fiber can be considered as independent. Eq. (5) can now be rewritten as follows:

$$N_d = \pi d_f(1+\eta) \int_0^{\lambda} \tau(u)du \tag{6}$$

Using the linear expression of $\tau(u)$ in terms of relative slip and initial bond strength between the fiber and concrete (τ_0) proposed by Lin and Li [15] after several arrangements, the pullout force of a single fiber in the debonding stage can be given by:

$$N_d(w) = \frac{\pi d_f}{2}\sqrt{E_f\tau_0 d_f(1+\eta)}\sqrt{w} \tag{7}$$

The corresponding width of the crack when all the embedded part is pulled out ($\lambda = L$), w_0, is approximated by:

$$w_0 \approx \frac{4(1+\eta)L^2\tau_0}{d_f E_f} \tag{8}$$

The debonding stage is completed on all fiber across the crack when these fibers with embedded length $L = L_f/2$ are all pulled out. The corresponding width of the crack (w_0) becomes w^* as follows:

$$w^* = \frac{(1+\eta)L_f^2\tau_0}{d_f E_f} \tag{9}$$

For the hooked-end steel fibers, when the width of the crack opening exceeds the critical value w_0, the straightening stage is triggered. The hooks are pulled straight due to the reaction at the bending points (see Fig. 2(b)). Assuming that the fiber slips as a rigid body through the bending point with the friction coefficient μ, *pulley friction* model [14] assumes the increased forces ($\Delta N_{L1,2}$) due to the straightening of hooks with the length of $L_{1,2}$ (see Fig. 1) are as follows:

$$\begin{aligned} \Delta N_{L1} &= Q = \frac{\pi f_y d_f^2}{12 \sin\psi \left[1 - \mu \sin(\psi/2)\right]^2} \\ \Delta N_{L2} &= \frac{Q}{2}\left(1 - \mu \sin\frac{\psi}{2}\right) \text{ where } f_y \text{ is the elastic limit of steel} \end{aligned} \tag{10}$$

To estimate the pullout force at the straightening stage, Alwan et al. [14] proposed two parabolic regimes for this stage. The first parabolic starts from $(N_d(w_0), w_0)$ to the peak $((N_d(w_0)+\Delta N_{L1}), L_1/2)$. The second one continues from this peak to the point of $(N_d(w_0) + \Delta N_{L2}, L_1 + L_2)$ (see Fig. 3). From this assumption, the straightening functions N_{re} and N_{ra} can be expressed by the following equations:

$$N_{re}(w) = -Q\left(\frac{w - w_0}{\frac{L_1}{2} - w_0}\right)^2 + 2Q\left(\frac{w - w_0}{\frac{L_1}{2} - w_0}\right) + \pi d_f(1+\eta)\tau_0 L; \quad \forall w \in \left(w_0, \frac{L_1}{2}\right] \tag{11}$$

$$N_{ra}(w) = -\frac{Q}{2}\left(1 + \mu \sin\frac{\psi}{2}\right)\left(\frac{w - L_1}{L_2}\right)^2 + Q + \pi d_f(1+\eta)\tau_0 L; \quad \forall w \in \left(\frac{L_1}{2}, L_1 + L_2\right] \tag{12}$$

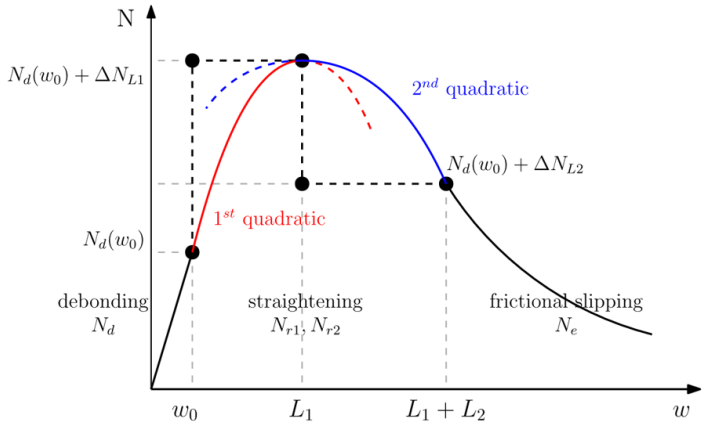

Figure 3. Pullout function at each stage (modified from [14])

When all the hooks of the fiber are straightened, the stress in the fiber has been relatively high and it may exceed the elastic limit f_y, the fiber undergoes the frictional slipping stage. Based on the method described in [15], the pullout force at this stage can be estimated as follows:

$$N_e(w) = \left[\pi d_f(1+\eta)\tau_0 L + \frac{Q}{2}\left(1 - \mu \sin\frac{\psi}{2}\right)\right]\left(1 - \frac{w - L_1 - L_2}{L}\right) \quad \forall w \in \left(L_1 + L_2, L_f/2\right] \tag{13}$$

2.2. *Description of the distribution of fiber orientation*

The fiber orientation is represented on spherical coordinate (r, φ, θ) with the principal axis $\vec{r}$ parallel with the normal of the crack plane (see Fig. 4). The relationship between the spherical coordinate and Descartes coordinate is presented by the following equation:

$$\begin{cases} x = r\cos\varphi\cos\theta \\ y = r\sin\varphi\sin\theta \\ z = r\cos\varphi \end{cases} \Leftrightarrow \begin{cases} r = \sqrt{x^2+y^2+z^2} \\ \varphi = \arccos\left(\dfrac{z}{\sqrt{x^2+y^2+z^2}}\right) \\ \theta = \arctan\left(\dfrac{y}{x}\right) \end{cases} \tag{14}$$

Due to the symmetric nature of the fiber to the crack plane, the distribution of fiber orientations can be considered on one-eighth of a sphere $(\varphi, \theta) \in [0, \pi/2] \times [0, 2\pi]$. In spherical coordinates, the distribution function $p_\varphi(\varphi, \theta)$ can be expressed following Gaussian-like probability density function of φ with period π as follows [25]:

$$p_\varphi(\varphi, \theta) = \cosh\left(k_g \cos\varphi\right) \tag{15}$$

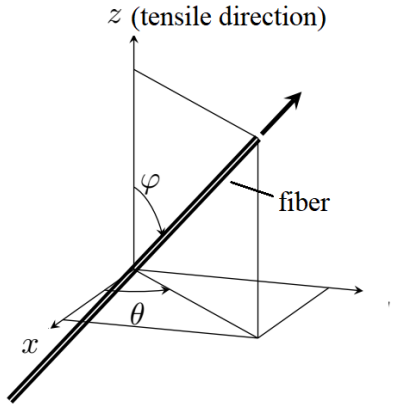

Figure 4. Fiber orientation in spherical coordinates

where k_g represents the dispersion of the distribution. The higher value of k_g implies the higher quantity of fiber oriented toward the average orientation. Let φ_0 be average orientation or reference orientation. Using the relationship between two coordinates (Eq. (14)) and normalizing it with the Jacobian of transformation, the probability density function (Eq. (15)) is rewritten in Descartes coordinates as follows:

$$p_\varphi(\varphi, \theta) = \frac{k_g}{2\pi \sinh k_g} \cosh\left[k_g(\cos\varphi\cos\varphi_0 - \sin\varphi\sin\theta\sin\varphi_0)\right]\sin\varphi \tag{16}$$

The cumulative value α of $p_\varphi(\varphi, \theta)$ over one-eighth of the sphere shows in Fig. 5. The value of α represents the probability of a fiber having the orientation φ within the set of fibers with the average orientation φ_0 and dispersion k_g. As displayed in Fig. 5: (i) for a given value of φ_0, when $k_g \to 0$, the value of $\alpha \to 0.5$; and (ii) for a fixed value of k_g, while the value of α increases when $\varphi_0 \to 0$, it decreases when $\varphi_0 \to \pm\pi/2$. This observation is suitable with the reported experimental results (e.g. [10–12]).

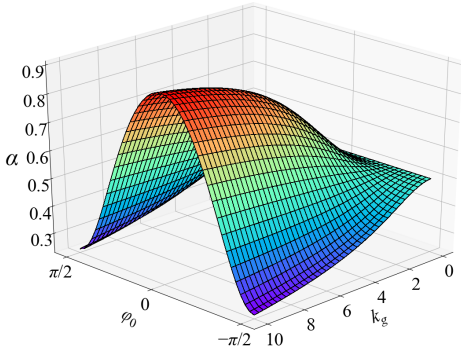

Figure 5. Relationship between the parameters (k_g, φ_0) of the fiber orientation distribution and the cumulative value of the density function α

In this study, for the analytical model, as the effect of segregation within concrete is neglected, the distribution of the fibers in the representative volume element can be assumed to be uniform. Therefore, the probability function of the relative position of the fibers to the crack can be calculated as follows:

$$p(z) = \frac{1}{L_f/2} = \frac{2}{L_f} \tag{17}$$

2.3. Behavior of SFRC at pre- and post-cracking

Based on the principles of the micromechanical model [21], for this study, the stress of the fiber at the crack (or the fiber bridging stress, $\sigma_f(w)$) can be expressed by the following equation:

$$\sigma_f(w) = \frac{v_f}{A_f}\int_{\theta=0}^{2\pi}\int_{\varphi=0}^{\pi/2}\int_{0}^{L} p(w,L)p(z)p_\varphi(\varphi,\theta)dLd\varphi d\theta \tag{18}$$

Applying the limitation conditions for the variables in Eq. (18), the bridging stress of the fiber $\sigma_f(w)$ for two types of the fibers are expressed as follows:

- *For hooked-end fiber:* with $z_d = \frac{L_f}{2} - \sqrt{\frac{E_f d_f}{4(1+\eta)\tau_0}w}$

(i) $\forall w \in [0, w^*]$:

$$\sigma_f(w) = \frac{8v_f}{\pi d_f^2 L_f}\left(\int_{\theta=0}^{2\pi}\int_{\varphi=0}^{\pi/2}\int_{z=0}^{z_d\cos\varphi} N_d(w,z,\varphi)p_\varphi(\varphi,\theta)dzd\varphi d\theta + \int_{\theta=0}^{2\pi}\int_{\varphi=0}^{\pi/2}\int_{z=z_d}^{\left(\frac{L_f}{2}-w\right)\cos\varphi} N_{re}(w,z,\varphi)p_\varphi(\varphi,\theta)dzd\varphi d\theta\right) \tag{19}$$

(ii) $\forall w \in \left(w^*, L_f/2\right]$:

$$\sigma_f(w) = \frac{8v_f}{\pi d_f^2 L_f}\int_{\theta=0}^{2\pi}\int_{\varphi=0}^{\pi/2}\int_{z=0}^{\left(\frac{L_f}{2}-w\right)\cos\varphi} N_{re}(w,z,\varphi)p_\varphi(\varphi,\theta)dzd\varphi d\theta \tag{20}$$

(iii) $\forall w \in (L_1/2, L_1 + L_2]$:

$$\sigma_f(w) = \frac{8v_f}{\pi d_f^2 L_f}\int_{\theta=0}^{2\pi}\int_{\varphi=0}^{\pi/2}\int_{z=0}^{\left(\frac{L_f}{2}-w\right)\cos\varphi} N_{ra}(w,z,\varphi)p_\varphi(\varphi,\theta)dzd\varphi d\theta \tag{21}$$

(iv) $\forall w \in \left(L_1 + L_2, L_f/2\right]$:

$$\sigma_f(w) = \frac{8v_f}{\pi d_f^2 L_f}\int_{\theta=0}^{2\pi}\int_{\varphi=0}^{\pi/2}\int_{z=0}^{\left(\frac{L_f}{2}-w\right)\cos\varphi} N_e(w,z,\varphi)p_\varphi(\varphi,\theta)dzd\varphi d\theta \tag{22}$$

- *For straight fiber:* with $z_d = \frac{L_f}{2} - \sqrt{\frac{E_f d_f}{4(1+\eta)\tau_0}w}$

(i) $\forall w \in [0, w^*]$:

$$\sigma_f(w) = \frac{8v_f}{\pi d_f^2 L_f}\left(\int_{\theta=0}^{2\pi}\int_{\varphi=0}^{\pi/2}\int_{z=0}^{z_d\cos\varphi} N_d(w,z,\varphi)p_\varphi(\varphi,\theta)dzd\varphi d\theta + \int_{\theta=0}^{2\pi}\int_{\varphi=0}^{\pi/2}\int_{z=0}^{\left(\frac{L_f}{2}-w\right)\cos\varphi} N_e(w,z,\varphi)p_\varphi(\varphi,\theta)dzd\varphi d\theta\right) \tag{23}$$

(ii) $\forall w \in \left(w^*, L_f/2\right]$:

$$\sigma_f(w) = \frac{8v_f}{\pi d_f^2 L_f}\int_{\theta=0}^{2\pi}\int_{\varphi=0}^{\pi/2}\int_{z=0}^{\left(\frac{L_f}{2}-w\right)\cos\varphi} N_e(w,z,\varphi)p_\varphi(\varphi,\theta)dzd\varphi d\theta \tag{24}$$

Prior to cracking, concrete shows a linear elastic behavior. Therefore, the stress of hardened concrete matrix in the pre-cracking can be expressed as follows:

$$\sigma_c = E_m\varepsilon_m = E_m\frac{\Delta l}{l_c} \tag{25}$$

where E_m and ε_m are the elastic modulus and the deformation of the cement matrix, respectively; Δl is the elongation; and l_c is called the characteristic length.

Finally, the constitutive behavior of SFRC is expressed through the combination of the stress of the hardened concrete matrix and the fiber bridging stress as follows:

$$\sigma(w) = \sigma_c H(f_t - \sigma_c) + \sigma_f(w) \tag{26}$$

where f_t is the tensile strength of the hardened concrete matrix, and H is the step-function defined as follows:

$$H(x) = \begin{cases} 1 & \forall x > 0 \\ 0 & \forall x \le 0 \end{cases} \tag{27}$$

3. Model appraisal

3.1. Parametric study

In this section, the variations of the constitutive model (Eq. (26)) with several parameters are investigated by using numerical programming in Python 3. For this work, three geometrical parameters of the fibers including the length of the fiber (L_f), the diameter of the fiber (d_f), and the dispersion coefficient of the density function (k_g), and one parameter of the material properties, the initial bonding stress (τ_0) are examined. To investigate the influences of these four parameters on the constitutive model, for a given category of L_f or d_f or τ_0, three values including the reference value shown in Table 1 and two values equal to 20% of the reference value were examined. In this study three values $k_g = 0.1; 8; 100$ were considered. $k_g = 8$ represents the coefficient of fiber orientation corresponding $\alpha = 0.75$ (see Fig. 5). This reference k_g-value is frequently observed in experimental works (e.g. [26, 27]). $k_g = 100$ implies that all fibers are oriented toward the average direction (φ_0), while $k_g = 0.1$ means the isotropic orientation. The reference values of all the input parameters used in this study are summarized in Table 1. Noted that except for the four parameters L_f, d_f, τ_0, and k_g, all the remaining parameters in Table 1 are kept unchanged for any analysis in this study.

For a given parameter, both hooked-end and straight fibers are considered (note that the lengths and angles of the hooks are null for straight fibers) The influences of the four examined parameters on the relationship between σ and w are presented in Fig. 6 to Fig. 9. Each figure contains a smaller figure at the top right conner that presents the variation of the curves up to the crack size of 0.3mm. Overall, all the four examined parameters significantly influence the model, however, the variation of the proposed model is relatively proportional. From the results shown in Fig. 6 to Fig. 9, some conclusions can be drawn:

(i) The cohesive stress of SFRC increases with increasing the fiber length (L_f) and the initial bond strength (τ_0) as well as the dispersion coefficient (k_g). These variations are consistent with the experimental results reported in [9, 28, 29].

(ii) The cohesive stress of SFRC decreases with increasing the diameter of the fiber (d_f).

Table 1. Input parameters for reference simulation

L_f (mm)	60.0
L_1 (mm)	2.9
L_2 (mm)	2.1
d_f (mm)	0.75
E_f (MPa)	210000
f_y (MPa)	1500
E_m (MPa)	35000
f_t (MPa)	3.5
v_f	0.005
μ	0.15
ψ (rad)	$\pi/4$
φ_0 (rad)	$\pi/6$
k_g	8.0

(iii) In straightening stage, the cohesive stress of SFRC used hooked-end fibers decreases with increasing the fiber length (L_f) (see Fig. 7(a)). Meanwhile, an opposite behavior is observed for SFRC used straight steel fibers (see Fig. 7(b)). This can be explained by the fact that in the straightening stage, the second quadratic function is used for the hooked-end fibers (see Fig. 3), while it is not used for the straight fibers.

Overall, it can be concluded that the proposed model behaves in a stable way with different values of the examined parameters

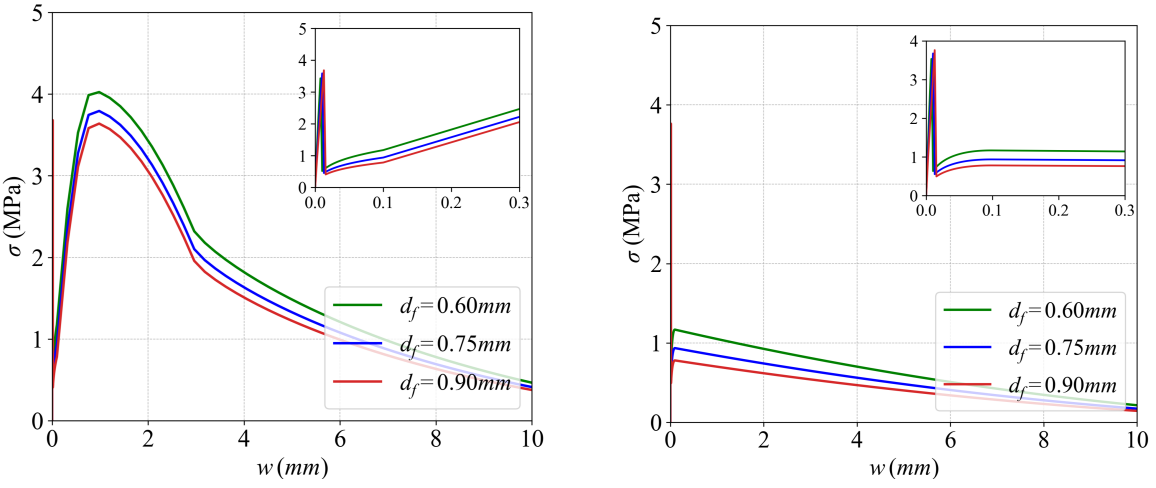

(a) Hooked-end fibers (b) Straight fibers

Figure 6. Influence of fiber diameter d_f on the relationship between σ and w

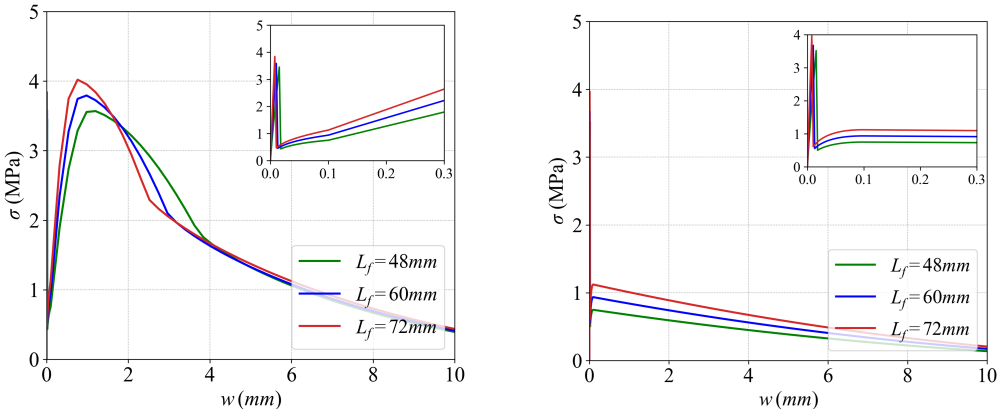

(a) Hooked-end fibers (b) Straight fibers

Figure 7. Influence of fiber length L_f on the relationship between σ and w

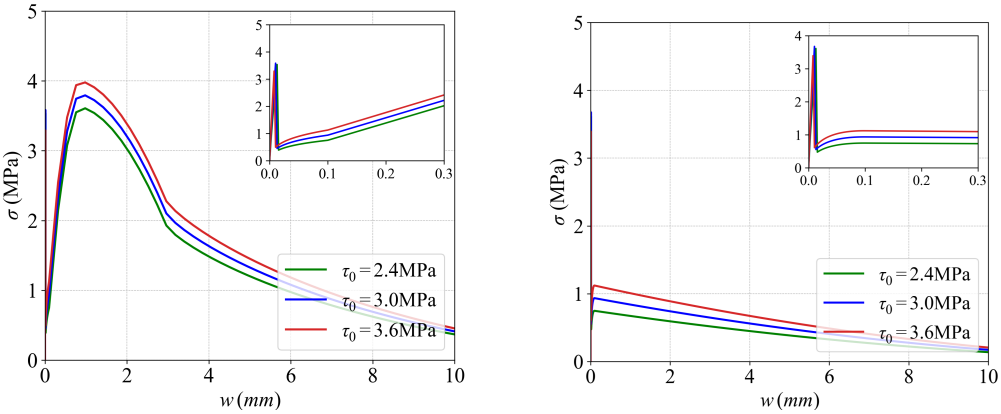

(a) Hooked-end fibers (b) Straight fibers

Figure 8. Influence of initial bond strength τ_0 on the relationship between σ and w

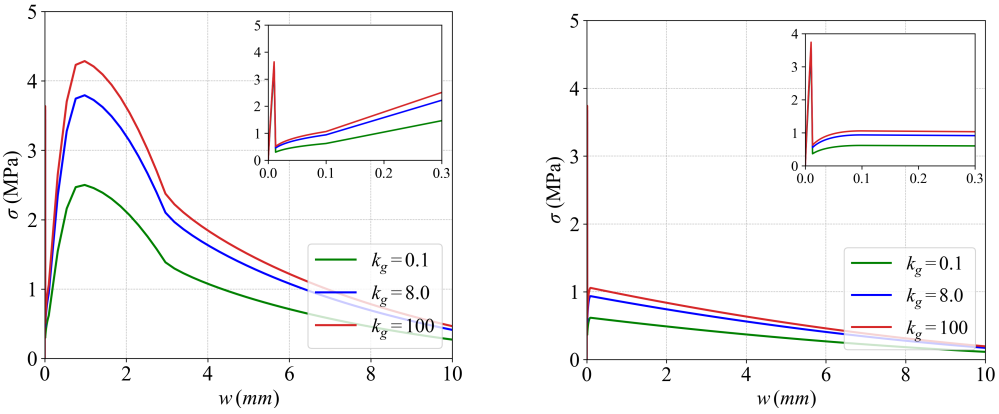

(a) Hooked-end fibers (b) Straight fibers

Figure 9. Influence of dispersion coefficient k_g on the relationship between σ and w

3.2. Model validation with experimental results

In order to verify the proposed model in practical situations, the numerical prediction is performed with the reported data of two uniaxial tensile tests on: (i) notched cylinder fabricated from regular SFRC [30]; and (ii) high-performance fiber reinforced concrete (HPFRC) with the pre-oriented straight fibers 8]

a. Regular SFRC with hooked-end fibers

Mudadu et al. [30] performed a series of direct tensile tests on notched cylinders with the diameter of 80 mm and the height of 160 mm. The cross-sectional area at the middle height of the cylinder is reduced by 10% to assure the cracks position (notched section). To measure the crack width (i.e., relative displacement between the two considered points symmetrically arranged around the notched section), three LVDTs (Linear Variable Differential Transformer) with a band of 40 mm are placed around the notched section (see Fig. 10).

The concrete used for this tensile test has the Young modulus E_m = 34 GPa and the compressive strength f_{cm} = 55 MPa. The tensile strength of hardened concrete matrix can be estimated following the empirical equation recommended in Eurocode 2 as: $f_t = 0.3 \times f_{cm}^{2/3} = 4.34$ (MPa). The initial bond strength can be chosen as equal to the tensile strength of hardened concrete matrix $\tau_0 = f_t$.

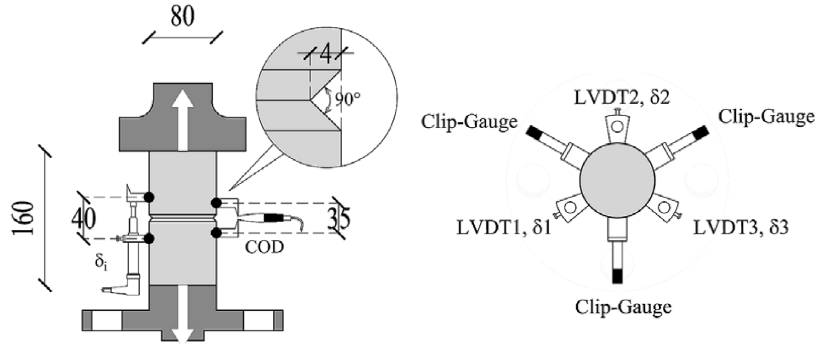

Figure 10. Illustration of testing setup for the direct tensile experiments [30] performed on notched SFRC cylinders (modified from [30])

The geometrical properties of the fiber are: L_f = 35 mm, $L_1 = L_2$ = 1.5 mm, and d_f = 0.55 mm. The elastic limit of steel fiber f_y = 1345 MPa. The characteristic length is chosen as the band width of LVDT l_c = 40 mm. Three fiber contents v_f = 0.3%, v_f = 0.5%, and v_f = 1.0% were tested. For a given of v_f, the corresponding spatial properties of the fibers α, φ_0, and k_g are summarized in Table 2.

Table 2. The volume fraction and the corresponding spatial properties of the fibers used in tensile tests of [30]

v_f	α	φ_0 (rad)	k_g
0.003	0.72	0.258	8.2
0.005	0.69	0.244	8.0
0.010	0.71	0.256	8.1

As shown in Fig. 11, the numerical model shows a reasonable estimation with the experimental results of [30], especially for the low fiber content. However, for the highest fiber content (v_f = 1.0%) the numerical model overestimates the bridging stress compared with the tested observation (see Fig. 11). This can be explained by the hypothesis of the present model that all fibers work independently until they are completely pulled out. Nevertheless, fibers that are close to each other have

certain interactions and become significant as the fiber content increases. This interaction can cause local damage to the hardened concrete matrix and the fibers can be pulled out before completing the sliding process.

b. High-performance fiber reinforced concrete with the pre-oriented straight fibers

In this section, a series of tensile tests on prisms fabricated from high-performance fiber reinforced concrete (HPFRC) using pre-oriented straight fibers of Bayard [8] is analyzed. To orient the fibers in the concrete sample, the author used several thin shells that were placed into the mold with a distance of 20 mm. These shells were then removed when finishing the casting process. The material properties and the geometrical parameters of the fibers used for these tests are listed in Table 3.

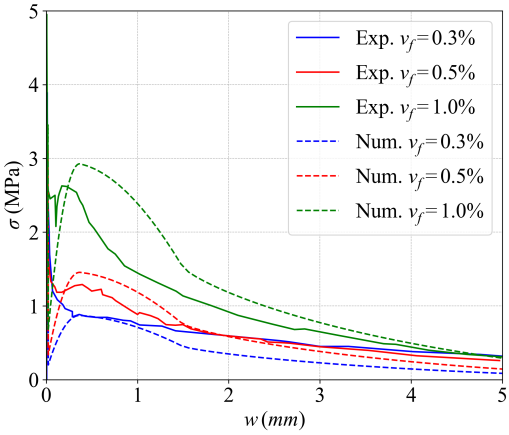

Figure 11. Comparison of numerical prediction with experimental observations of direct tensile test on notched SFRC cylinder reported in [30]

Table 3. Material properties and geometrical parameters of the fibers used in the direct tensile tests of [8]

L_f (mm)	d_f (mm)	E_f (MPa)	f_y (MPa)	v_f	E_m (MPa)	f_t (MPa)	τ_0 (MPa)
13.0	0.20	210000	1800	0.027	45000	7.0	7.0

For the casting process described above, the dispersion of fiber orientation can be assumed as small. Hence, it can be assumed $k_g = 8.0$ that is an average value frequently observed in reported experiments (see section 3.1) and this value was applied for all numerical simulations in the present study.

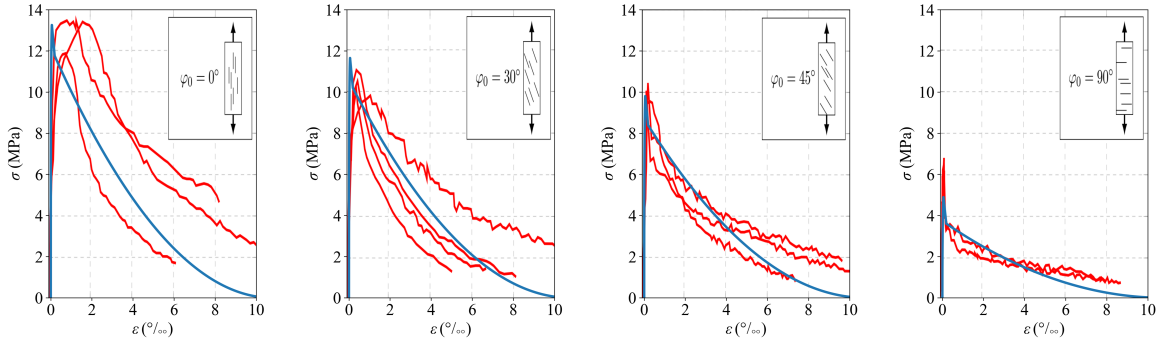

(a) (b) (c) (d)

Figure 12. Comparisons of numerical prediction (blue curve) with experimental results (set of red curves) of direct tensile tests on HPFRC with the pre-oriented straight fibers performed in [8]

As displayed in Fig. 12, the proposed prediction model presents a good agreement with the experimental results. However, for the proposed model, the strain hardening stage seems to be slightly underestimated compared with the experimental results. In other words, the model does not allow for accurate estimation of the nonlinear hardening behavior of materials at small deformation. This

can be explained by the fact that the HPFRC samples were not notched. Hence, the microcracks can be distributed throughout the samples. It then causes a long strain-hardening stage and leads to the formation of numerous macrocrack. Meanwhile, the present numerical model considers only one macrocrack perpendicular to the direction of the applied load (see Fig. 2). However, all simulated curves fall within the range of the experimental results, and the critical post-cracking stress can be estimated quite accurately by the present numerical model.

4. Conclusions

In this paper, a numerical model is developed to predict the cohesive stress at post-cracking stage of steel fiber reinforced concrete considering the fiber orientation. In this model, the fiber bridging stress is introduced as an analytical function of material properties. The combination of the "pulley friction" model and the "elastic hardening" model introduced in this paper allows to present the work of both straight fiber and hooked-end fiber. The distribution of fiber orientation is represented through a new Gaussian-like -periodic density function

Parameter studies performed in the present work show that the proposed model provides quite consistent results with experimental observations. Simulations on two cases of direct tensile tests also show a reasonably good estimation of the model for the cohesive stress after cracking. The proposed distribution function of fibers orientation has proven to be effective in representing the uneven distribution of fibers orientation. However, the model has a certain deviation in the case of hooked fibers and with a relatively high fiber content, that requires a further study on the effect of the interaction of the fibers within the hardened concrete matrix.

Although there are still some limitations, the proposed model has a lot of potential for development. For instance, the bridging stress function can be directly used for cohesive elements in local finite element models, or used as a function to calculate energy released rate in global finite element models when cracking occurs.

References

[1] Bentur, A., Mindess, S. (2006). *Fibre reinforced cementitious composites*. CRC Press.

[2] Hoan, P. T., Thuong, N. T. (2019). Shear resistance of ultra-high-performance concrete reinforced with hybrid steel fiber subjected to impact loading. *Journal of Science and Technology in Civil Engineering (STCE) - NUCE*, 13(1):12–20.

[3] Thao, N. T. T., Tung, T. P. S., Nhan, N. D., Tan, N. N. (2022). Assessing the shear behavior of steel fiber reinforced concrete beams corroded under chloride attacks. *Journal of Science and Technology in Civil Engineering (STCE) - HUCE*, 16(3):97–110.

[4] Tan, N. N., Thao, N. T. T., Van, N. T., Hieu, D. D. (2022). Assessing the shear behavior of corroded steel fiber reinforced concrete beams without shear reinforcement using nonlinear finite element analysis. *Journal of Science and Technology in Civil Engineering (STCE) - HUCE*, 16(3):152–165.

[5] Casanova, P., Rossi, P., Schaller, I. (1997). Can steel fibers replace transverse reinforcements in reinforced concrete beams? *ACI Materials Journal*, 94(5):341–354.

[6] Cucchiara, C., Mendola, L. L., Papia, M. (2004). Effectiveness of stirrups and steel fibres as shear reinforcement. *Cement and Concrete Composites*, 26(7):777–786.

[7] Rossi, P. (1998). Bétons de fibres métalliques (BFM). *Les superstructures du bâtiment*.

[8] Bayard, O. (2003). Approche multi-échelles du comportement mécanique des bétons à ultra hautes performances renforcés par des fibres courtes. PhD thesis, Cachan, Ecole normale supérieure.

[9] Behloul, M. (1996). Analyse et modélisation du comportement d'un matériau à matrice cimentaire fibrée à ultra hautes performances: bétons de poudres réactives, du matériau à la structure. PhD thesis, Cachan, Ecole normale supérieure.

[10] Barros, J. A. O., Cunha, V. M. C. F., Ribeiro, A. F., Antunes, J. A. B. (2005). Post-cracking behaviour of steel fibre reinforced concrete. *Materials and Structures*, 38(1):47–56.

[11] Chanvillard, G. (1992). *Analyse expérimentale et modélisation micromécanique du comportement des fibres d'acier tréfilées, ancrées dans une matrice cimentaire*. Laboratoire Central des Ponts et Chaussées.
[12] Robins, P., Austin, S., Jones, P. (2002). Pull-out behaviour of hooked steel fibres. *Materials and Structures*, 35(7):434–442.
[13] Naaman, A. E., Shah, S. P. (1976). Pull-out mechanism in steel fiber-reinforced concrete. *Journal of the Structural Division*, 102(8):1537–1548.
[14] Alwan, J. M., Naaman, A. E., Guerrero, P. (1999). Effect of mechanical clamping on the pull-out response of hooked steel fibers embedded in cementitious matrices. *Concrete Science and Engineering*, 1(1):15–25.
[15] Lin, Z., Li, V. C. (1997). Crack bridging in fiber reinforced cementitious composites with slip-hardening interfaces. *Journal of the Mechanics and Physics of Solids*, 45(5):763–787.
[16] Zhang, J., Li, V. C. (2002). Effect of inclination angle on fiber rupture load in fiber reinforced cementitious composites. *Composites Science and Technology*, 62(6):775–781.
[17] Yang, E.-H., Wang, S., Yang, Y., Li, V. C. (2008). Fiber-bridging constitutive law of engineered cementitious composites. *Journal of Advanced Concrete Technology*, 6(1):181–193.
[18] Wu, C., Leung, C. K. Y., Li, V. C. (2018). Derivation of crack bridging stresses in engineered cementitious composites under combined opening and shear displacements. *Cement and Concrete Research*, 107:253–263.
[19] Carvalho, M. R., Barros, J. A. O., Zhang, Y., da Costa, D. D. (2020). A computational model for simulation of steel fibre reinforced concrete with explicit fibres and cracks. *Computer Methods in Applied Mechanics and Engineering*, 363:112879.
[20] Tailhan, J.-L., Rossi, P., Daviau-Desnoyers, D. (2015). Probabilistic numerical modelling of cracking in steel fibre reinforced concretes (SFRC) structures. *Cement and Concrete Composites*, 55:315–321.
[21] Li, V. C., Wang, Y., Backer, S. (1991). A micromechanical model of tension-softening and bridging toughening of short random fiber reinforced brittle matrix composites. *Journal of the Mechanics and Physics of Solids*, 39(5):607–625.
[22] Ng, T. S., Foster, S. J., Htet, M. L., Htut, T. N. S. (2013). Mixed mode fracture behaviour of steel fibre reinforced concrete. *Materials and Structures*, 47(1-2):67–76.
[23] Voo, J. Y. L., Foster, S. J. (2003). Variable engagement model for the design of fibre reinforced concrete structures. In *Advanced Materials for Construction of Bridges, Buildings, and Other Structures*, volume III.
[24] Zhan, Y., Meschke, G. (2016). Multilevel computational model for failure analysis of steel-fiber–reinforced concrete structures. *Journal of Engineering Mechanics*, 142(11).
[25] Breitenberger, E. (1963). Analogues of the normal distribution on the circle and the sphere. *Biometrika*, 50(1-2):81–88.
[26] Gettu, R., Gardner, D. R., Saldívar, H., Barragán, B. E. (2005). Study of the distribution and orientation of fibers in SFRC specimens. *Materials and Structures*, 38(1):31–37.
[27] Blanco, A., Pujadas, P., de la Fuente, A., Cavalaro, S. H. P., Aguado, A. (2015). Assessment of the fibre orientation factor in SFRC slabs. *Composites Part B: Engineering*, 68:343–354.
[28] Tue, N. V., Henze, S. (2008). Determination of the distribution and orientation of fibres in steel fibre reinforced UHPC by photographic method. In *Ultra High Performance Concrete (UHPC)*, Kassel, Germany, 505–512.
[29] Laranjeira de Oliveira, F. (2010). Design-oriented constitutive model for steel fiber reinforced concrete. PhD thesis, Universitat Politècnica de Catalunya.
[30] Mudadu, A., Tiberti, G., Germano, F., Plizzari, G. A., Morbi, A. (2018). The effect of fiber orientation on the post-cracking behavior of steel fiber reinforced concrete under bending and uniaxial tensile tests. *Cement and Concrete Composites*, 93:274–288.